Laser-Induced Phosphorescence for the in Situ Detection of Glyoxal at Part per Trillion Mixing Ratios

ARTICLE *in* ANALYTICAL CHEMISTRY · AUGUST 2008

Impact Factor: 5.64 · DOI: 10.1021/ac800407b · Source: PubMed

7 AUTHORS, INCLUDING:

Andrew Huisman
University of Wisconsin–Madison
25 PUBLICATIONS **231** CITATIONS
SEE PROFILE

Joshua P. Digangi
Princeton University
9 PUBLICATIONS **210** CITATIONS
SEE PROFILE

Melissa M Galloway
Lafayette College
40 PUBLICATIONS **504** CITATIONS
SEE PROFILE

Anal. Chem. **2008,** *80,* 5884–5891

Laser-Induced Phosphorescence for the in Situ Detection of Glyoxal at Part per Trillion Mixing Ratios

Andrew J. Huisman, John R. Hottle, Katherine L. Coens, Joshua P. DiGangi, Melissa M. Galloway, Aster Kammrath, and Frank N. Keutsch*

Department of Chemistry, University of Wisconsin—Madison, 1101 University Avenue, Madison, Wisconsin 53706

Glyoxal is a molecule of emerging importance to the atmospheric chemistry community because of its role in aerosol formation and utility as an indicator for oxidative chemistry. We describe the Madison laser-induced phosphorescence (LIP) instrument, an instrument based on LIP for direct, in situ measurement of gas-phase glyoxal with a S/N = 3 limit of detection (LOD) of 18 ppt_v/min, with planned upgrades to reduce the LOD to 5 ppt_v/min. By employing this technique, we have built an instrument with exceptional in situ limits of detection, tremendous selectivity, and the considerable advantage of direct, fast measurements that requires neither derivatization nor ex situ analysis. The instrument is equally well-suited for laboratory and field measurements. It was deployed for the first time to the BEARPEX 2007 field campaign in Georgetown, CA, producing nearly one month of continuous data with mixing ratios ranging from 20 to 250 ppt_v glyoxal. To the authors' knowledge, this represents the first use of LIP for a field measurement.

Glyoxal (GL), the smallest α-dicarbonyl, has recently gained the interest of the atmospheric chemistry community. Because its primary emissions are negligible,[1] GL observed in the atmosphere is justifiably correlated to oxidative chemistry. Specifically, GL is produced by OH radical-initiated oxidation of anthropogenic aromatic volatile organic compounds (VOCs),[2] alkenes and acetylene, reactions of O_3 with alkenes,[3] and the oxidation of biogenic molecules such as isoprene and 2-methyl-3-buten-2-ol.[4,5] Thus, the observation of GL concentrations and trends can be used as a metric for the overall oxidative chemical processes of both anthropogenic and biogenic VOCs occurring in the atmosphere. Because of its short lifetime (see below), GL is especially promising in the study of local, small-scale processes. Further, GL contributes to the formation of secondary organic aerosol (SOA)[6,7] and has been proposed as an indicator of SOA formation.[8]

The atmospheric chemistry and fate of atmospheric GL is under study by a number of groups and has recently begun to see use in global atmospheric chemistry models (viz. GEOS-Chem[4] or TM4[9]) and in photochemical box models.[3] It has a lifetime against solar photolysis of ~2 h in overhead sun[10] and a lifetime against oxidation by OH-radical of ~6 h.[11] Recent work suggests that wet and dry deposition of GL are relatively minor sinks, with estimates ranging from less than 1% to over 10%[3,9] of total loss processes. Despite a high vapor pressure (~50 Torr at 0 °C),[12] GL has been shown to partition to the aerosol phase several orders of magnitude more strongly than its Henry's law constant would suggest,[7] and recent evidence indicates that partitioning to the aerosol phase becomes the predominant sink under high aerosol conditions, reducing the lifetime of GL to ~40 min.[3]

Efforts to understand the role of GL and its utility to atmospheric processes are hampered by the low mixing ratios at which it typically occurs, especially in rural or remote regions, making fast, accurate measurements difficult or impossible. Indirect measurements in nonurban settings are in the range of 0−600 ppt_v, with the majority falling in the range of 0−200 ppt_v.[4] Volkamer et al. used differential optical absorption spectroscopy (DOAS) to directly measure mixing ratios up to 1.8 ppb_v in Mexico City in 2005,[1] while Sinreich et al. reported values ranging from 40 to 140 ppt_v for Cambridge, MA, and 50−430 ppt_v for a deployment to the Gulf of Maine using MAX-DOAS.[13] The 2006 SCIAMACHY GL satellite retrievals showed the unexpected result

* To whom correspondence should be addressed. E-mail: keutsch@wisc.edu.

(1) Volkamer, R.; Molina, L. T.; Molina, M. J.; Shirley, T.; Brune, W. H. *Geophys. Res. Lett.* **2005**, *32*, L08806.
(2) Volkamer, R.; Platt, U.; Wirtz, K. *J. Phys. Chem. A.* **2001**, *105*, 7865–7874.
(3) Volkamer, R.; San Martini, F.; Molina, L. T.; Salcedo, D.; Jimenez, J. L.; Molina, M. J. *Geophys. Res. Lett.* **2007**, *34*, L19807.
(4) Fu, T.-M.; Jacob, D. J.; Wittrock, F.; Burrows, J. P.; Vrekoussis, M. J. Geophys. Res. In press.
(5) Grosjean, D. *Environ. Sci. Technol.* **1990**, *24*, 1428–1432.
(6) Liggio, J.; Li, S.-M.; McLaren, R. *J. Geophys. Res.* **2005**, *110*, D10304.
(7) Kroll, J. H.; Ng, N. L.; Murphy, S. M.; Varutbangkul, V.; Flagan, R. C.; Seinfeld, J. H. *J. Geophys. Res.* **2005**, *110*, D23207.
(8) Volkamer, R.; Jimenez, J. L.; San Martini, F.; Dzepina, K.; Zhang, Q.; Salcedo, D.; Molina, L. T.; Worsnop, D. R.; Molina, M. J. *Geophys. Res. Lett.* **2006**, *33*, L17811.
(9) Myriokefalitakis, S.; Vrekoussis, M.; Tsigaridis, K.; Wittrock, F.; Richter, A.; Brühl, C.; Volkamer, R.; Burrows, J. P.; Kanakidou, M. *Atmos. Chem. Phys. Discuss.* **2008**, *8*, 1673.
(10) Volkamer, R.; Spietz, P.; Burrows, J.; Platt, U. *J. Photochem. Photobiol. A: Chem.* **2005**, *172*, 35–46.
(11) Feierabend, K. J.; Zhu, L.; Talukdar, R. K.; Burkholder, J. B. *J Phys Chem A* **2008**, *112*, 73–82.
(12) Dobeck, L. M.; Lambert, H. M.; Kong, W.; Pisano, P. J.; Houston, P. L. *J. Phys. Chem. A.* **1999**, *103*, 10312–10323.
(13) Sinreich, R.; Volkamer, R.; Filsinger, F.; Frieβ, U.; Kern, C.; Platt, U.; Sebastián, O.; Wagner, T. *Atmos. Chem. Phys.* **2007**, *7*, 1293–1303.

10.1021/ac800407b CCC: $40.75
Published on Web 07/02/2008

of elevated GL mixing ratios over some open oceans, while the EOS Aura's ozone monitoring instrument had retrievals showing low GL in the same regions but elevated GL in areas influenced by continental biomass burning; it is clear that satellite retrievals will require further validation to reach their full utility.[14,15] Altogether, high sensitivity and direct measurements of GL are a priority because of its apparent utility as a tracer for atmospheric oxidative processes and SOA formation and because of the need for satellite validation and model intercomparison.

Currently, the only direct measurements of glyoxal employ the DOAS technique, with a reported sensitivity of 150 ppt_v in 2−15 min^1 for measurements of glyoxal in addition to other species. Neglecting duty cycle spent aligning and changing spectral features, the sensitivity is 150 ppt_v/10 s for long path-DOAS[3] and 40 ppt_v/30 s for MAX-DOAS[13] measuring only glyoxal. While the sensitivity of long path-DOAS cannot be improved by longer averaging, it may be increased by a longer light path, and there is the potential to improve the MAX-DOAS sensitivity by a factor of 4.[16] DOAS techniques have the advantage of measuring multiple species over a long fetch, which is more suited to making representative measurements of inhomogeneous air parcels, while the method described herein and derivatization methods are point measurements. Derivatization of gaseous GL with 2,4-dinitrophenylhydrazine and subsequent detection by LC−mass spectrometry has been successfully employed to measure GL in ambient air both on the ground and in airborne instrumentation: 65 ppt_v in 1 min for 5-min samples for aircraft instruments,[17] and 328 ppt_v in 1 min for 2-h samples for ground instruments.[18] For ease of comparison, limits of detection (LOD) are reported in 1-min data rates as S/N = 3, assuming that other instruments' LOD scale as the square root of sampling time when possible. This class of measurement has acceptable to poor temporal resolution but the considerable advantage of measuring multiple compounds simultaneously.[18] However, it is nonideal in that it is an indirect measurement and may suffer from both positive and negative interferent effects from atmospheric ozone.[19] Recent derivatization studies employing *O*-(2,3,4,5,6-pentafluorobenzyl)hydroxylamine as the derivatizing agent report excellent limits of detection (7.5 ppt_v in 1 min for 10-min samples) and reduced ozone interference,[19] but still require indirect detection, limiting their ability to detect fast features in atmospheric GL. As GL is emerging as a tracer of local photochemistry, an instrument for its measurement should have both high temporal and spatial resolution. This is especially true if an instrument is to be made airborne, where spatial and temporal resolution are directly related.

The importance of GL as a tracer of photochemistry, in models, and for satellite retrieval validation indicates the need for accurate measurements with good spatial and temporal resolution. In this paper, we present and characterize an instrument that meets this need. Glyoxal is detected via LIP using the Madison LIP Instrument. The technique is highly sensitive, permitting specific, direct, in situ measurement of GL with a 1-min limit of detection near the predicted global background of 10 ppt_v.[4] The instrument was deployed for the first time to BEARPEX 2007, at a research site located on a ponderosa pine plantation in the foothills of the Sierra Nevada, ∼50 miles east of Sacramento, CA. The site, on Sierra Pacific Industries land, is at an elevation of 4000 ft and is near the Blodgett Forest Research Station, which is operated by the College of Natural Resources and the Department of Environmental Science and Policy Management of the University of California, Berkeley. While deployed, it operated autonomously for days at a time, producing nearly one month of continuous data with mixing ratios ranging from 20 to 250 ppt_v glyoxal. Using the 3σ method of determining sensitivity and taking the noise over a period of nighttime data in which GL was changing very little, we calculate the minimum detectable limit for this instrument is 18 ppt_v/min. Unless otherwise noted, all data presented come from this deployment. Procedures are described for the periodic calibrations required by the instrument, as is the extensive intracalibration telemetry used to track any changes in detection efficiency. To the authors' knowledge, this represents the first use of LIP for a field measurement.

EXPERIMENTAL SECTION

The key to the Madison LIP instrument lies in the fact that glyoxal has a near-unity triplet yield ($^3A_u \leftarrow {}^1A_u$) at moderate total pressures ($P > 1$ Torr).[20] The $8_0^1\ {}^1A_u \leftarrow X^1A_g$ transition to the S_1 ^1A_u state ($\sigma_{GL} > 10^{-18}$ cm^2/molecule) is excited near 440 nm (22 715 cm^{-1}), and the system undergoes complete and nearly instantaneous conversion to the T_1 ^3A_u state, which phosphoresces with a lifetime on the order of 10 μs in 100 Torr air,[21] driven by the quenching of T_1 GL by O_2 ($k = 0.0030 \pm 0.0001$ μs^{-1} $Torr^{-1}$).[22] This lifetime is sufficiently long to permit complete isolation of the GL phosphorescence signal from all instantaneous and fast interferences (Rayleigh, Raman, and particle scatter, as well as fluorescence of interferents) via gated detection, as described in the Data Analysis section below. Furthermore, the distinct rotational structure[23] of the $8_0^1\ {}^1A_u \leftarrow X^1A_g$ band shown in Figure 1 provides a convenient means of accounting for fluctuations in background, also described in the Data Analysis section below.

The design of the LIP instrument is analogous to that of the Harvard[24,25] and Berkeley[26] NO_2 LIF instruments. The entire instrument can be described in four subunits: (a) excitation laser system, (b) detection cell, (c) gas flow (including calibration gas), and (d) data acquisition and control.

(a) Laser System. A novel, custom, high-resolution ($\Delta\tilde{\nu}_{FWHM} < 0.04$ cm^{-1} at 440 nm) doubled Ti:sapphire laser (Photonix

(14) Wittrock, F.; Richter, A.; Oetjen, H.; Burrows, J. P.; Kanakidou, M.; Myriokefalitakis, S.; Volkamer, R.; Beirle, S.; Platt, U.; Wagner, T. *Geophys. Res. Lett.* **2006**, *33*, L16804.
(15) Kurosu, T. P.; Volkamer, R.; Fu, T.-M.; Millet, D.; Chance, K.
(16) Volkamer, R. Personal communication, 2008.
(17) Lee, Y.-N.; Zhou, X.; Leaitch, W. R.; Banic, C. M. *J. Geophys. Res.* **1996**, *101*, 29075.
(18) François, S.; Perraud, V.; Pflieger, M.; Monod, A.; Wortham, H. *Atmos. Environ.* **2005**, *39*, 6642–6653.
(19) Spaulding, R. S.; Talbot, R. W.; Charles, M. J. *Environ. Sci. Technol.* **2002**, *36*, 1798–1808.
(20) Anderson, L. G.; Parmenter, C. S.; Poland, H. M. *Chem. Phys.* **1973**, *1*, 401–417.
(21) Huisman, A. J.; Bootsma, S. J.; Keutsch, F. N. In preparation.
(22) Yardley, J. *J. Chem. Phys.* **1972**, *56*, 6192–6197.
(23) Co, D. T. Unpublished material, 2006.
(24) Perkins, K. K.; Hanisco, T. F.; Cohen, R. C.; Koch, L. C.; Stimpfle, R. M.; Voss, P. B.; Bonne, G. P.; Lanzendorf, E. J.; Anderson, J. G.; Wennberg, P. O.; Gao, R. S.; Del Negro, L. A.; Salawitch, R. J.; McElroy, C. T.; Hintsa, E. J.; Loewenstein, M.; Bui, T. P. *J. Phys. Chem. A* **2001**, *105*, 1521–1534.
(25) Perkins, K. K. In situ observations of nitrogen dioxides using laser-induced fluorescence detection: Examining the nitrogen oxides - nitric acid system in the lower stratosphere. Ph.D. Dissertation, Harvard University, Cambridge, MA, 2000.
(26) Thornton, J. A.; Wooldridge, P. J.; Cohen, R. C. *Anal. Chem.* **2000**, *72*, 528–539.

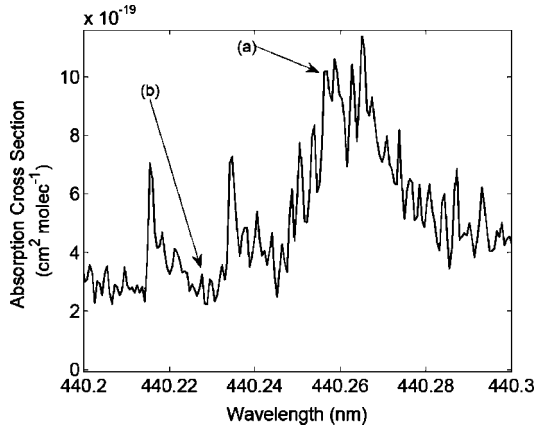

Figure 1. High-resolution cross section of glyoxal. The high resolution cross section of GL[23] showing rotational structure. The laser is dithered between (a) an "online" position on the broad peak near 440.26 nm and (b) an "offline" position near the relatively flat region at 440.23 nm.

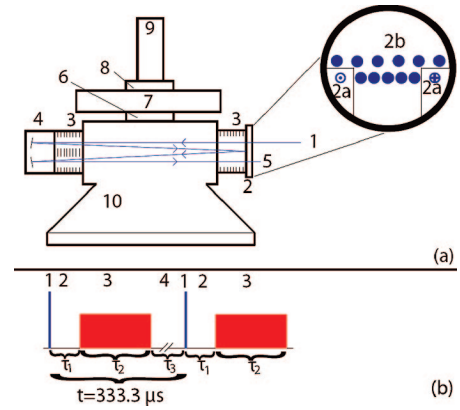

Figure 2. White cell optical assembly schematic. Panel a schematically depicts the parts of the white cell, including the multipass pattern (inset): The input beam (1) enters the cell through a cutout in the entrance mirror (2a). It forms a multipass pattern between the twin mirrors (4) and the entrance mirror (2b), passing through optical baffles (3), which reduce scatter. It exits (5) through another cutout in the entrance mirror (2a). Detection is accomplished by the photon counting PMT (9) after passing through the filter changer (7) with accompanying optics (6, 8). Background is reduced by a light trap (10). Panel b illustrates the temporal resolution of the gated photon counting. The laser (1) is followed by ~1.7 μs of noncounting region (2). Signal is then collected for 37.5 μs (3) and rejected from the remainder of the duty cycle (4) to further reduce background.

Industries, Bohemia, NY) was modified by the addition of a custom piezo rotation stage (Physik Instrumente, Karlsruhe/Palmbach, Germany) with subnanometer position control to allow very precise, highly reproducible, rapid control of the laser wavelength. The laser and all other instrumental components are controlled by custom software written in LabVIEW 8.1 (National Instruments, Austin, TX). The doubled output of a diode pumped Nd:YAG at 532 nm is used to pump a Ti:sapphire crystal with a fundamental wavelength near 880 nm, which is in turn doubled to produce coherent 440-nm light, with precise tuning accomplished by rotating a diffraction grating (mounted on the custom piezo rotation stage), which acts as one of the cavity mirrors. The laser is operated at a repetition rate of 3000 Hz, producing 80-mW average power (30-ns fwhm pulses) centered at 440.25 nm (22714 cm^{-1}) with a tuning range of 8 cm^{-1}, limited by the fine-tuning range of the piezo rotation stage. The laser power is monitored immediately after the laser unit using a 95/5 beam sampler (ThorLabs BSF05-A1, Newton, NJ) and a power meter (Melles Griot 13PEM001/J, Longmont, CO) or a UDT-555UV photodiode (OSI Optoelectronics, Hawthorn, CA). After generation by the laser, light is steered with Edmund Optics 48015 turning mirrors (Barrington, NJ) and fiber coupled (115 ft CDI2264, Thor Laboratories) to the detection axis. Wherever possible, antireflection coated optics are used.

(b) Detection Cell. Gas flows through a White-type multipass cell (analogous to the Harvard NO_2 cell[25]), which is operated at either 32 or 40 passes and is optically baffled by aluminum baffles blackened with a mixture of carbon black (Sigma-Aldrich) and Alion MH-2200 (Alion Science and Technology, McLean, VA) to reduce background. This equipment has been adapted from the Madison HCHO LIF instrument.[27] Of glyoxal's several phosphorescence bands, the 520-nm band was chosen for its strong signal, spectral separation from the 440-nm excitation wavelength (for efficient filtering of scattered laser light), and availability of high quantum efficiency detectors. An imaging lens (CVI Laser, Carlsbad, CA, biconvex diameter 38.1 mm, ROC_1 = 100 CX, ROC_2 = 30.988 CX) restricts the field of view of the detector to ~1 cm^3 in the center of the detection volume (see Figure 2). The application of a custom, high-transmission 520-nm (fwhm transmission 20 nm, 75% peak transmission) bandpass filter (Barr Associates, Westford, MA) before the photon counting PMT (Electron Tubes P25PC-03, 15% Q.E. at 520 nm, Rockaway NJ) allows highly selective and highly sensitive detection: neither unfiltered ambient air at 60% relative humidity nor NO_2 in mixing ratios exceeding 1 ppm_v cause any discernible interference. Therefore, no filtering of the analyte gas for particulates or water vapor is required. The P25PC-03 photon counter operates linearly up to count rates of 1×10^7 counts s^{-1}; no corrections were undertaken as all data from the test deployment were at rates less than 5×10^4 counts s^{-1}. A 490-nm bandpass filter (Semrock, Inc. FF01-488/6-25, Rochester, NY) designed to capture only N_2 Raman scatter is periodically substituted for the 520-nm bandpass to monitor changes in collection efficiency. A swinging-arm type filter changer is used, following the design of Thornton et al.[26] Slight ultra zero air (UZA) (Airgas Inc.) purges, totaling 200 sccm, are used to prevent the dead volume of the light trap and the optics mounts from influencing the gas turnover rate and to keep the optics clean.

(c) Gas Flow and Calibration. Ambient air is drawn through the inlet to a 100 SLM flow controller (MKS Instruments type 1559A, Andover, MA), passed through the cell (see Figure 3), and exhausted by a scroll pump (BOC Edwards XDS35i, Wilmington, MA). The white cell, including fiber coupling and power monitor optics, is mounted to a 0.5-in. aluminum plate, forming a single module, which facilitates movement and alignment. Wherever possible, PTFE or PFA tubing and parts are used and the cell and inlet tubing are heated to 35 °C to minimize loss of analyte. Nominal conditions are ~38 SLM main flow through the 100 SLM controller at 100 Torr cell pressure as measured by a Baratron 722A capacitance manometer (MKS Instruments) attached to a

(27) Hottle, J. R.; Huisman, A. J.; Coens, K. L.; DiGangi J. P.; Galloway, M. M.; Kammrath, A.; Keutsch, F. N. *Environ. Sci. Technol.* Submitted.

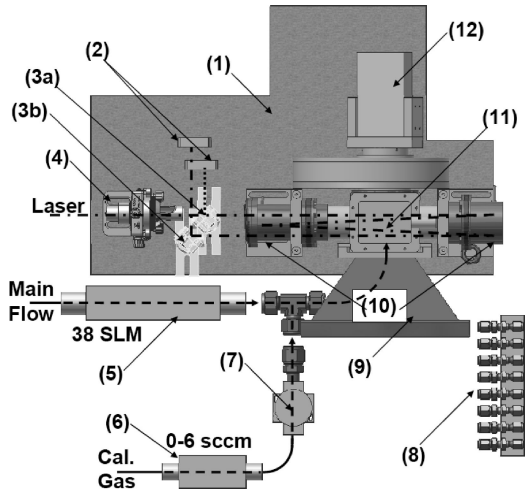

Figure 3. Gas flow schematic. The white cell is permanently mounted to a 0.5-in. aluminum optical surface [textured] (1). The laser (dash−dotted line) arrives at the tower via a fiber-optic and fiber coupler (4), which is used to align the beam into the cell. The beam power is monitored by photodiodes (2), with a beam sampler (3a) to monitor power in and a mirror (3b) dumping the outgoing beam on the photodiode. The main flow (38 SLM) is controlled by a 100 SLM flow controller (5) and enters the cell through a flange directly under the marker (11). Calibration gas is controlled by a 10 sccm flow controller (6) with an all-Teflon wetted positive shutoff valve (7). A gas manifold (8) supplies UZA for purges on the light trap (9) and optics (10). The output flange (11) connects to vacuum. The PMT and filter changer (12) are shown for reference.

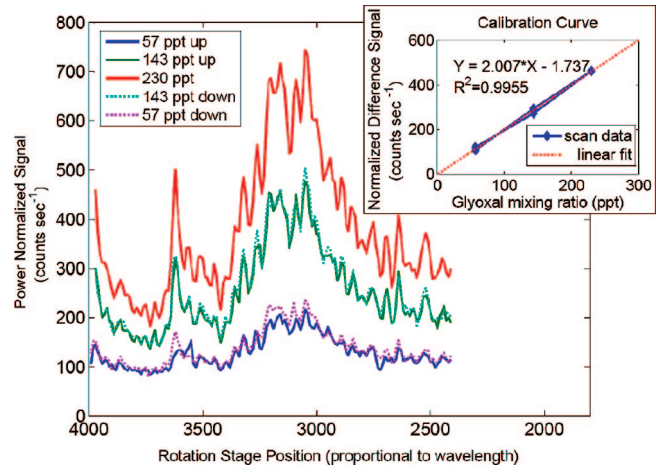

Figure 4. Calibration data showing multiple scans. The labels "up" and "down" denote the rising and falling concentration limbs of the scan sequence (which were 57, 143, 230, 143, and 57 ppb_v), which was so ordered to check for hysteresis. Inset: the normalized difference signal from which the calibration is established. This configuration shows very little offset (−1.737 ppt_v at zero counts) and a calibration factor of ~0.5 power-normalized difference counts per second per ppt_v glyoxal.

shunt on the body of the cell. Calibration gas is periodically introduced through a 10 sccm flow controller (MKS Instruments type 1779A) with a positive shutoff valve with all-Teflon wetted parts (Parker SV-2-1144-2, Cleveland, OH).

The pronounced tendency of GL to be taken up into the condensed phase not only has implications for SOA formation but also demands particular care in handling of standard gases for calibration of the LIP cell. Gas-phase GL is produced from the trimer dihydrate (Sigma Aldrich) following the P_2O_5 method outlined in Kroll et al.[7] and is diluted with UZA into a thoroughly dried 12-L glass bulb to a mixing ratio of ~1 ppm_v. The bulb is stored in a dark box at all times. The mixing ratio of GL in the bulb is determined by measuring the absorbance of the mixture with cavity-ringdown absorption spectroscopy (see, for example, Zalicki et al.[28]), following the NOAA NO_3 ringdown cell design,[29,30] and using 99.995% high reflector cavity mirrors (901-0010-0440 HR cavity mirrors, Los Gatos Research, Mountain View, CA). Detection is accomplished by a Hamamatsu H5783 PMT using a custom >100-MHz amplifier and a 100-MHz data acquisition card (GaGe Applied Technologies Compuscope 14100, Lockport, IL), with fitting by a proprietary fast ringdown fitting algorithm (Greg Engel, University of Chicago). The known absorption cross sections near the 8^1_0 band[10] are used to determine the GL mixing ratio. This same bulb is then treated as a calibration standard, and this gas flows into the LIP cell to directly calibrate the system and ensure that the laser is locked onto the spectral feature of interest. Ringdown measurements are performed on each bulb before the bulb is used for the first time and after the bulb is removed from the instrument to account for any changes in the standard gas over time. Calibration factors were stable within 20% over the course of the field mission, but no calibrations are available during the second two weeks of field validation because the standard gas was compromised, possibly as a result of lower temperatures at the time.

Before using the standard gas to calibrate the LIP cell, the tubing to the bulb is flushed three times with small amounts of the standard gas. The main flow is held at the nominal 38 SLM of ambient air to maintain pressure in the cell. A short tube (4 ft 0.25-in.-o.d. PTFE) connects the standard gas to the gas handling system (cf. Figure 3). After starting or changing the calibrant flow, the signal is monitored and is considered stabilized after it is constant for at least 30 s. Typical stabilizing times were less than 2 min. LIP measurements are taken at flows of 2, 4, 6, 4, and 2 sccm (see Figure 4) to account for any hysteresis in the system, effectively a variation on the method of standard additions, which precludes offsets due to GL in ambient air. This method was employed to most fully replicate experimental conditions and because it was impractical to use UZA for the main flow during calibrations because of the high flow rates. The rising and falling concentration limbs of the calibration sequence yielded nearly identical results, implying no discernible hysteresis. These LIP cell calibrations are performed only at night, when the ambient GL concentration is not expected to vary quickly in time, an inference that is borne out by measurements of night-time GL concentrations.

To minimize wall loss, the main flow inlet is made as short as possible. However, it was not possible to harden some critical equipment for outdoor operation. To this end, the instrument is designed modularly, with a "ground" unit consisting of the laser, wavemeter, and control and support electronics fiber coupled to a "tower" unit with the White cell, photon counting PMT, and

(28) Zalicki, P.; Zare, R. *J. Chem. Phys.* **1995**, *102*, 2708–2717.
(29) Dube, W. P.; Brown, S. S.; Osthoff, H. D.; Nunley, M. R.; Ciciora, S. J.; Paris, M. W.; McLaughlin, R. J.; Ravishankara, A. R. *Rev. Sci. Instrum.* **2006**, *77*, 034101.
(30) Osthoff, H. D.; Brown, S. S.; Ryerson, T. B.; Fortin, T. J.; Lerner, B. M.; Williams, E. J.; Pettersson, A.; Baynard, T.; Dubé, W. P.; Ciciora, S. J.; Ravishankara, A. R. *J. Geophys. Res.* **2006**, *111*, D12305.

gas flow equipment. In this way, the detection axis can be placed in a location that would otherwise be inaccessible (for example, 12 m above ground level on a tower during field testing at BEARPEX 2007) because of the sensitive nature of the laser and support electronics.

(d) Data Acquisition and Control. The heart of the experiment is the photon counting PMT, which is used to detect GL phosphorescence. Special care was taken to faithfully transmit the signal (5 V, 10 ns TTL square pulse) from the "tower" to the "ground" unit. Short lengths (6 ft) of RG-58 coaxial cable were used to connect to the main transmission line, 115 ft of RG-8U coaxial cable. Laboratory experiments before deployment showed that the signal was moderately attenuated by transmission. Over 90% of signal pulses are counted, a ratio that remains stable throughout operation. Because both calibrations and measurements were taken in this configuration, the dropped counts do not result in a signal offset. The instrument is interfaced to the computer through all-custom printed circuit boards connected directly to a pair of PCI-6221 multifunction data acquisition boards (National Instruments). The photon counter signal is acquired using the counter/timer on one of the boards. All other signals are generated or measured using the digital I/O, analog in and analog out channels of the same boards. These signals are carried on separate, shielded cables (115 ft), which are bundled by signal type to avoid cross talk. Static digital and analog out signals are carried on Belden 9519 38 conductor wire, while analog in signals are carried on Belden 8342 25 conductor wire, using the twisted pairs as signal and signal ground for differential measurement. A separate, shielded serial cable is used to communicate with a custom-designed printed circuit board carrying 8 thermistors (Murata Electronics NTSD1WC303FPB50, Smyrna, GA), which monitors the temperature of equipment in the "tower" portion. The cell and inlet are heated to 35 °C, using foil heaters (Minco Heaters, Minneapolis, MN) to reduce analyte wall loss, and held within a range of ±1.5 °C by a simple software feedback loop that controls the power to the heaters based on the thermistor readings.

The phosphorescence signal (TTL logic, 10 ns high time) is routed to an edge counter on the PCI-6221 running in gated counting mode. A second 80-MHz counter on the same PCI-6221 is used to generate the gate, which is controlled in delay and width by the computer and triggered by the laser pulse. All counts arriving outside this gate are rejected at the counter, effectively removing any laser scatter or other fast ($<\sim$1.5 μs) processes. The gate settings are discussed below. The instrument is able to operate at nearly 100% counter duty cycle by taking many of the necessary telemetry measurements in the background while the counter is accumulating. These include beam power at the laser, as well as the power before and after the cell, and the pressure, gas flows, and temperature of the components. The ratio of power before and after the cell is an excellent metric for the quality of alignment. The absolute laser wavelength is monitored with a pulsed wavemeter at 1 Hz (Bristol Instruments, Victor, NY). The cell pressure and actual gas flow rates are recorded at 1 Hz, while the temperatures of the components as reported by the thermistors are recorded at 0.1 Hz.

Although the counter operates at nearly 100% duty cycle, measurements of ambient air are taken at only ~85% duty cycle and consist of dithering the excitation wavelength between the maximum of the spectral feature at 440.26 nm (cf. Figure 1) and a nearby minimum at 440.23 nm (henceforth referred to as "online" and "offline"). Data are collected in 1-s bins for 40 s online, followed by 20 s offline for background purposes. The wavelength change, accomplished with the piezo-driven rotation stage, is instantaneous on the time scale of the measurements (20 ms including settling time).

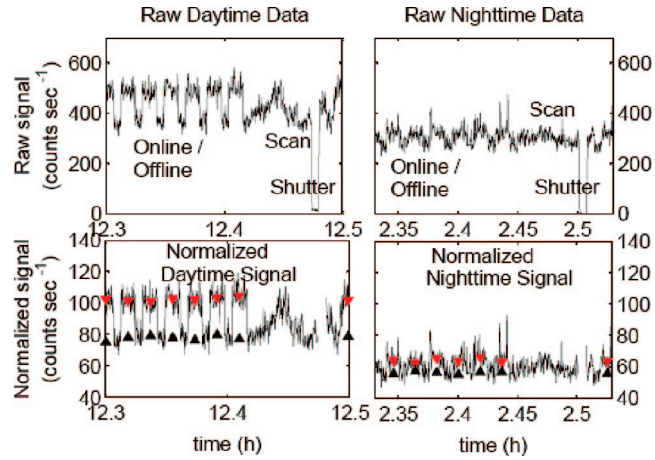

Figure 5. Raw data. The raw data streams from daytime and nighttime, including a scan over the peak region and data collected with the laser shuttered. Note that both the top (unnormalized) and bottom (normalized) sets have the same vertical scale. The 1-min averaged data are shown as triangles on the lower set. The difference between these values is proportional to the amount of GL measured.

The remaining ~15% of the duty cycle is occupied with additional telemetry. Every half hour, instead of dithering online to offline, a complete scan over the peak region (440.2−440.3 nm) is collected to ensure that the laser wavelength has not drifted away from the spectral feature of interest. A secondary offline, which may be used to account for nonfeatureless background counts, is monitored every 10 min. Additionally, data are collected for 20 s with the laser shuttered to monitor dark counts and light leaks, which might result in zero offsets. Finally, the N_2 Raman scatter filter can be substituted for the GL phosphorescence filter to monitor changes in collection efficiency.

SIGNAL PROCESSING

Phosphorescence counts are collected in 1-s bins (corresponding to 3000 laser shots) and postprocessed to 1-min average data. The raw 1-Hz data are normalized by laser power, and the online signal for each 1-min interval is defined as the simple average of each 40-s segment, while the offline processed signal was taken as the average of the last 10 s of the preceding offline segment and the first 10 s of the following offline segment. Because conditions at Blodgett Forest Research Station were unusually dry and dusty, dust occasionally resulted in spurious data lasting less than 5 s, so any 1-s bin lying more than three standard deviations away from the mean was rejected and the mean recalculated without it. Typical daytime and nighttime data are shown in Figure 5: the top frames show raw data from dithering online and offline, followed by a scan over the whole peak, and shuttering the laser, before returning to dithering online and offline. The bottom frames show the power normalized data, with the 1-min averaged data superimposed as triangles. A typical data set for one day is

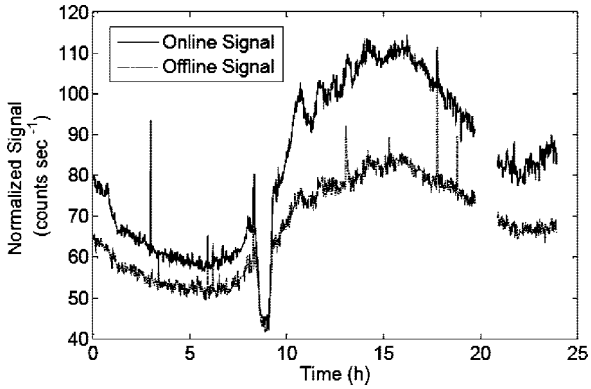

Figure 6. Online/offline difference data. Raw data streams showing the "online" and "offline" signals corresponding to the power normalized counts originating from the strong and weak absorption of GL. The pronounced dip around 9 h was a zeroing test, where ultra zero air was used as the main flow. Another interesting feature is the rapid increase in concentration around 10 a.m. The large spikes are removed by a 20-min bin 3-standard deviation criterion.

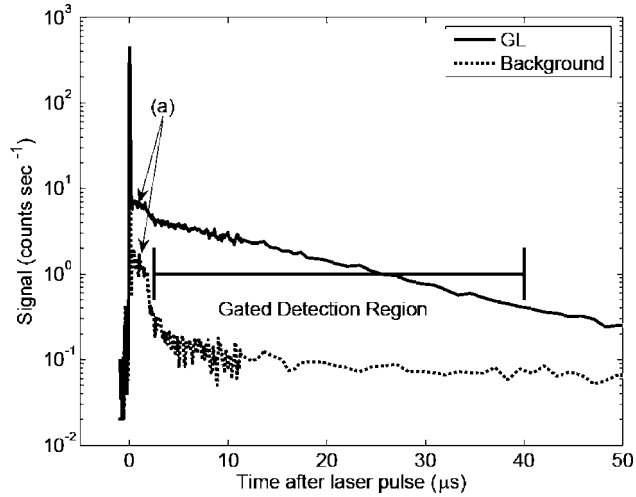

Figure 7. Gate settings. A 100 Torr cell pressure laboratory experiment showing the decay of signal following the laser pulse both with and without the addition of glyoxal. The e-folding time of the glyoxal signal is calculated to be ~15 μs and the gated detection region excludes all fast scatter as well as fast scatter or fluorescence processes, such as that of feature a.

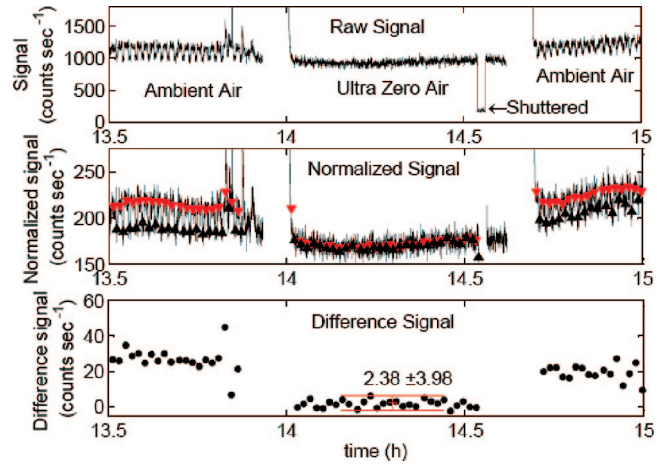

Figure 8. Ultra zero air zeroing test. Data showing an UZA zeroing of the instrument, including data before and after the test. Raw counts are shown in the top panel. The power-normalized signal is shown in the center panel, with 1-min averaged data shown as triangles. The difference signal is shown in the bottom panel.

presented in Figure 6. The penultimate signal is obtained by subtracting the average offline value from the average online value for a single 1-min period, yielding power-normalized difference data, which is proportional to the concentration of GL and is insensitive to broadband background by virtue of that subtraction. The final step is to multiply by a calibration factor, which is obtained by performing the same online−offline analysis on a sample of known GL mixing ratio (see Experimental Section part c above). Over the course of a day, the online and offline data are nominally continuous, validating the use of a 20-min moving average to smooth the data by removing points selected by a 3 standard deviation criterion. Less than 1% of points were removed in this way.

The cell pressure and gate parameters were optimized during precampaign laboratory experiments. Using an 80-MHz counter from the NI PCI-6221 (12.5-ns resolution) with a 60-ns bin size, the temporally resolved emission profile was recorded using a constant bulk flow of UZA with and without the addition of a small amount of GL gas flowing through the cell. The functional form of the with-glyoxal signal approaches a double exponential (see Figure 7), which is assumed to arise as a result of fast scatter processes and slower GL phosphorescence. The characteristic time of the phosphorescent signal shows a marked dependence on pressure, ranging from an e-folding time of ~160 μs at 10 Torr to ~15 μs at 100 Torr. Lower pressures have higher phosphorescence yields (leading to higher signal rates) and longer ^3A_u lifetimes, resulting in a signal that is more fully resolved from the laser pulse,[22] but also have reduced overall signal due to the lower GL number density. In the end, an operating pressure of 100 Torr was used with a gate of width 37.5 μs delayed 1.7 μs from the laser pulse as shown in Figure 7. It is worth noting that small variations in gate and delay (±10%) and of the pressure (±5 Torr) have little effect on detection limit and accuracy.

Field Validation. Several tests were performed to characterize the instrument in a field environment at BEARPEX 2007. Characterization of the inlet was performed in an attempt to understand what effect, if any, it had on the signal. First, periodic zeros were taken by using UZA as the bulk flow (see Figure 8). Upon introduction of the UZA as main flow, the difference signal dropped to less than 10% of its former value. A slight zero offset is apparent, corresponding to a mixing ratio of 15 ppt$_v$, below the 1-min limit of detection and quite low in comparison to typical daytime mixing ratios of 100−250 ppt$_v$. It is possible that this offset was the result of contamination of the cell, which had been calibrated with gas-phase glyoxal three days previously. The detection axis heaters were activated two days before this UZA zeroing test, so that the measurement was performed on a heated cell while the calibration was not. The inlet (25 ft 0.5-in.-o.d. PTFE), which was used for ambient air, was used to plumb the UZA to the cell, also a possible source of this minor contamination. Future work will include more frequent UZA zeroings with a dedicated line and will have a consistently heated cell, allowing us to address this issue.

Second, the longer inlet tube (25 ft 0.5-in.-o.d. PTFE) was coiled, used while unheated, then heated to ~35 °C over its length

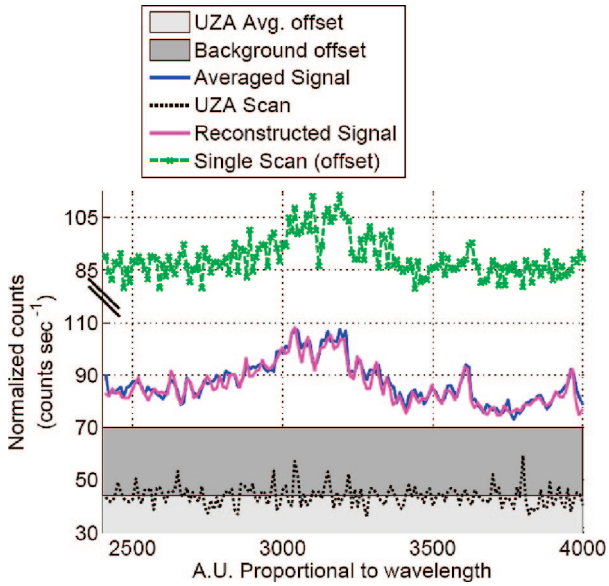

Figure 9. Analysis of ambient signal. The averaged signal from several daytime scans over the peak region clearly shows the glyoxal excitation spectrum (cf. Figure 1). This signal is already discernible in a single 1-Hz, 160-point scan (vertically offset for clarity) and is fully accounted for by adding a scaled absorption cross section of glyoxal (not shown) to the UZA and another featureless background.

under nominal flow conditions (38 SLM ambient air). No increase in phosphorescence signal was observed at the elevated inlet temperatures, implying that there was no thermally mediated reversible wall loss and that diurnal temperature cycles were not influencing the inlet characteristics. Third, the pump speed was modulated while maintaining pressure in the cell, inducing changes in the main flow rate. No difference in signal was observed, implying that neither absorption nor desorption of GL was occurring on the walls or inlet. Finally, a long (~100 ft) section of polyethylene tubing was used in place of the regular length (3 ft) PTFE inlet, to no apparent effect. On the basis of these observations, we conclude that the inlet material or length had little impact on the measured concentration of GL. Despite this, the inlet was kept as short as possible. Because all inlet tests were carried out under dry conditions (RH < 30%) and especially in light of work that suggests glyoxal will not condense to the aerosol phase at RH < 26%,[31] further studies are planned to fully characterize the inlet with respect to changes in humidity that might cause the inlet tubing to affect the analyte or interferent mixing ratios.

The rotation stage, which controlled the laser wavelength, was found to be stable for several days at a time during the campaign but was reset to the spectral feature of interest whenever a GL spectrum was available. Such a spectrum was definitively available during calibrations and was also frequently observed by scanning the laser over the spectral feature while drawing ambient air. The averaged signal (see Figure 9) from six scans over the peak region can be fully accounted for using only (1) the average offset observed during UZA zeroing, (2) an additional featureless (wavelength-independent) offset, and (3) the scaled glyoxal absorption cross section at 100 Torr (the cell operating pressure).

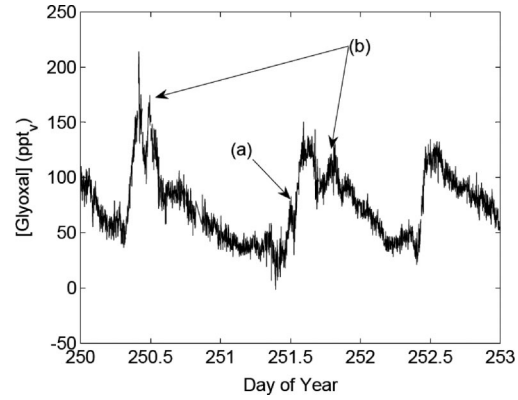

Figure 10. Sample data. Sample field data from day of year (DOY) 250 to DOY 253 at BEARPEX 2007. (a) shows a peak tentatively assigned to breakup of the boundary layer; (b) shows fast features near noon that may indicate local transport and photochemistry.

The UZA zeroing background from a single scan is shown for reference, but was assumed to be featureless (light gray box), and the glyoxal absorption cross section was scaled to reproduce the difference in peak height in the observed signal. The value for the additional featureless offset (dark gray box) was determined empirically to be ~125 counts s^{-1} (~25 normalized counts s^{-1}). Because both background offsets are wavelength-independent, they are subtracted during analysis (cf. Data Analysis section). In laboratory experiments (i.e., interferent-free conditions), the literature absorption cross section maps directly to the excitation spectrum taken with the LIP instrument. In that the field LIP signal directly reflects the absorption cross section, we have shown that there are no processes competing with transfer of excited S_1 glyoxal to the phosphorescent T_1 state.

A portion of the data from the campaign is shown in Figure 10. The laser power throughout operation was ~8 mW at the cell entrance, with typical count rates of 900 difference counts s^{-1} ppb^{-1} and typical glyoxal mixing ratios ranging from 20 to 250 ppt$_v$. It is worth noting that typical raw count rates for the field campaign of 1000−1500 counts s^{-1} correspond to less than 1 signal photon per laser pulse.

It is apparent that fluctuations in the concentration of GL have several fast components that would have been averaged out in a less sensitive measurement with lower temporal resolution. A few of these features bear closer examination: (a) shows a ~10-min peak that may be related to the morning breakup of the boundary layer, reflecting the increase in emissions and photochemistry and the increasing height of the boundary layer, both of which are driven by the sun. Feature b illustrates fast changes in mixing ratio that appear to be correlated to fast photochemistry of precursors, including isoprene and MBO, as well as other tracers of biogenic oxidative chemistry such as peroxymethyacrylic nitrate (data not shown); these data may be convoluted by transport processes. Overall, the GL mixing ratio is generally higher and the diurnal cycle is more pronounced than in the work of Spaulding et al. from the same site in another year.[32] Another paper examining the scientific merit of these data, including

(31) Hastings, W. P.; Koehler, C. A.; Bailey, E. L.; De Hann, D. O. *Environ. Sci. Technol.* **2005**, *39*, 8728.

(32) Spaulding, R. S.; Schade, G. W.; Goldstein, A. H.; Charles, M. J. *J. Geophys. Res.* **2003**, *108*, 4247.

correlations with concentrations of other molecules of interest, and the effects of transportation of precursors and GL is in preparation.[33]

CONCLUSION

We report the first use of a laser-induced phosphorescence field technique to measure gas-phase glyoxal, a molecule of emerging importance to atmospheric chemists and modelers. The sensitivity of this instrument (3σ) is 18 ppt_v/min. A number of tests confirm that the observed signal during the BEARPEX 2007 campaign arose from glyoxal in the ambient air, not as the result of reversible uptake or interferents. Planned upgrades to the instrument include a high quantum efficiency (40% at 520 nm) photon counting PMT (H7421-40, Hamamatsu Photonics, Bridgewater, NJ) and increasing the laser power to the full 80 mW, which should increase the sensitivity of this instrument to <5 ppt_v/min. Increased automation of telemetry, including automatic periodic UZA instrument zeroing and N_2 Raman data, will improve the reliability of the data. This instrument is also very well suited for laboratory and chamber experiments and could be converted into an instrument suitable for tropospheric airborne measurements by hardening against vibration and temperature changes. The sensitivity of the Madison LIP Instrument has the potential to increase our level of scientific understanding of atmospheric oxidative processes of VOCs and to provide valuable data that can be used to validate satellite retrievals and increase the accuracy and predictive capabilities of tropospheric chemistry models.

(33) Huisman, A. J. In preparation.

ACKNOWLEDGMENT

The author gratefully acknowledges the support of the University of Wisconsin—Madison Department of Chemistry, including especially Dr. R. McClain, and the research groups of Dr. F. Crim and Dr. J. Wright. The author acknowledges the noteworthy contributions of Dr. S. Brown, Dr. D. Co, and Dr. G. Engel. Field validations were carried out at Blodgett Forest Research Station on Sierra Pacific Industries property at BEARPEX 2007 with the help and support of staff and collaborators there. This work was supported by the National Science Foundation, Division of Atmospheric Sciences, Atmospheric Chemistry Program under Grant 0724912, and the NDSEG-ARO.

Received for review February 27, 2008. Accepted May 6, 2008.

AC800407B